Ice-induced vibrations and ice buckling

Hendrikse, Hayo; Metrikine, Andrei

DOI
10.1016/j.coldregions.2016.09.009

Publication date
2016

Document Version
Accepted author manuscript

Published in
Cold Regions Science and Technology

Ice-induced vibrations and ice buckling

Hayo Hendrikse[a,b,1], Andrei Metrikine[a,b]

[a] *Delft University of Technology, P.O. Box 5048, 2600GA, Delft, The Netherlands*
[b] *SAMCoT, Dep. Civil and Transport Engineering, NTNU, NO0-7491 Trondheim, Norway*

For final version see: http://dx.doi.org/10.1016/j.coldregions.2016.09.009

ABSTRACT

Ice-induced vibrations can occur when flexible, vertically-sided offshore structures are subject to level ice such that the failure mode of ice is predominantly crushing. When the ice is relatively thin, or when the width of the structure is much larger than the ice thickness, the ice tends to buckle and subsequently fail as soon as the stress caused by the buckling exceeds the bending strength of the ice sheet. This type of failure is referred to in this paper as buckling failure. The buckling failure can limit the global load on the structure but not necessarily prevents the development of ice-induced vibrations. Study of the latter in cases when ice fails by mixed crushing and buckling is of interest for the design of offshore structures as well as for the interpretation of model-scale tests which often show buckling as a consequence of the use of relatively thin ice. In this study a phenomenological approach for ice crushing and a model of a wedge beam on elastic foundation are combined, thereby composing a simplified model which incorporates both crushing and flexural motion of the ice sheet. Typical load signals and a failure mode map generated with the model correspond well with model-scale observations in a qualitative sense. The model predicts that ice-induced vibrations of limited duration can develop as long as the buckling failure does not occur within at least one period of intermittent crushing or frequency lock-in. A specific case is discussed for which buckling failure would be expected to occur, but sustained intermittent crushing is observed instead, illustrating that buckling does not necessarily limit the development and duration of ice-induced vibrations, but even the opposite could happen. The possibility for ice-induced vibrations to develop in the regime of mixed crushing and buckling failure is further discussed focusing on the effects of the boundary conditions, structural shape and structural and ice properties.

Keywords: *ice engineering; ice loads; ice-induced vibrations; ice-structure interaction; ice buckling*

1. INTRODUCTION

Flexible, vertically-sided offshore structures may experience ice-induced vibrations in level ice conditions for which the ice fails in crushing. Three regimes of ice-induced vibrations are distinguished, defined as intermittent crushing, frequency lock-in, and continuous brittle crushing (ISO19906, 2010). Often, in model-scale as well as full-scale conditions, ice-induced vibrations are limited in duration due to failure of ice in out-of-plane bending (Bjerkås et al., 2013; Ziemer and Evers, 2014). For vertically-sided structures the latter is often a result of buckling of the ice sheet that leads to large out-of-plane deformations. We refer to this type of failure as buckling failure, not to confuse it with bending failure observed when level ice acts on sloping structures or ship hulls.

Combined buckling and crushing of ice against vertically-sided structures occurs when the ice is relatively thin or the aspect ratio, defined as the ratio between structure width and ice thickness, is high (Kärnä and Jochmann, 2003; Timco, 1991). Such conditions may be present during significant part of the lifetime of offshore structures placed in locations where level ice is present. It is therefore of interest to model the scenario in which ice fails by mixed crushing and buckling, and study the possibility for ice-induced vibrations to develop within this scenario.

Existing phenomenological models and approaches for the study of ice-induced vibrations generally consider only crushing to occur (Kärnä et al., 1999; Määttänen, 1999; Sodhi, 1994). As such these models are applicable only to relatively thick ice and small aspect ratios.

In this paper we expand one of the most recent phenomenological models for ice crushing (Hendrikse and Metrikine, 2015) by combining it with a model of a wedge beam on elastic foundation. The resulting model

[1] Corresponding author. *Fax:* (+31) (0)15 2785767. *E-mail addresses:* H.Hendrikse@tudelft.nl (H. Hendrikse), A.Metrikine@tudelft.nl (A.V. Metrikine)

incorporates, in a simplified manner, creep, crushing, and flexural ice behaviour and captures typical trends observed for ice-induced vibrations. The wedge beam approach has been introduced by Kerr (1978) to be a reasonable approximation for the ice buckling problem taking into consideration the radial cracks which form in the ice during its interaction with a structure. Limitations of the wedge beam approach are discussed by Sodhi (1979) in comparison with plate theory. Although the limitations are quite severe, accuracy of the wedge beam model predictions is deemed sufficient for the developed phenomenological model. The model introduced in this paper is subsequently applied to study the development of ice-induced vibrations in the regime of mixed crushing and buckling. To the knowledge of the authors, studies on ice-induced vibrations in this regime are not available in the literature.

The paper is structured as follows. Section 2 briefly summarizes observations of and literature on failure modes which can occur when level ice acts on vertically-sided structures; some definitions are also introduced therein. Section 3 presents a description of the developed phenomenological model and the method of definition of input parameters. In Section 4 the model is applied to study action of a sheet of model-ice on a rigid, vertically-sided structure. The obtained results are discussed with reference to model-scale experimental observations. Section 5 presents a study of the development of ice-induced vibrations of a flexible structure in the regime of mixed crushing and buckling. Discussion of the obtained results and main conclusions are collected in Section 6 and Section 7.

2. FAILURE OF LEVEL ICE ACTING ON VERTICALLY-SIDED STRUCTURES

In this section we present a brief overview of ice failure as observed in model-scale and full-scale and specify some definitions used in this paper. Level ice acting on a vertically-sided structure may fail in multiple ways depending on indentation velocity, aspect ratio, and ice properties (Blanchet et al., 1988; Timco, 1991). In this paper we use the terms creep, crushing failure, and buckling failure as generalized terms each of which combines several deformation and crack formation processes in the ice. In Figure 1 the different crack formation processes are sketched, indicating which are encompassed by creep, crushing failure, and buckling failure. A failure map indicating the dependence of failure on indentation velocity and aspect ratio based on model-scale data from Timco (1991) is also shown to illustrate the transition between different types of failure. Typical time dependencies of the ice load for the different types of failure can be found in Timco (1987). We now briefly describe creep, crushing failure, buckling failure, and the transition between those.

Creep defines the deformation of ice at low indentation velocities and low aspect ratios, sometimes also referred to as ductile failure. Creep is characterized by full contact between the ice and structure and a uniform pressure at the ice-structure interface. Large creep deformations can develop over long periods of time. In creep the ice load increases gradually over time towards a peak value, after which the load reduces to a steady-state value (Sodhi, 1991). Creep of ice is treated in detail in Ponter et al. (1983) and Schulson and Duval (2009).

Crushing defines the ice deformation and failure at high indentation velocities and low aspect ratios which is characterized by local contacts and quasi-random ice load signals (Jordaan, 2001; Sodhi, 2001). We use the term crushing to define the combined pulverization of ice, formation of spalls and flakes, and formation of radial cracks. Spalls and flakes generally occur for aspect ratios above one, the range of interest for ice-induced vibrations, resulting in a wedge shaped front of the ice when looking from the side. Radial crack formation results in a wedge shaped geometry of the ice in front of the structure when looking from above, but does not necessarily have a measurable effect on the load on the structure (Palmer et al., 1983). Deformation of ice during crushing is mainly elastic at high indentation velocities. At indentation velocities around the transition from creep to crushing ‘ductile’ deformation, i.e. viscoelastic and/or plastic deformation, contributes to the total deformation, but the ice still fails by fracturing locally.

Buckling is defined as the out-of-plane deformation of the ice sheet resulting in failure as soon as the bending stress caused by the buckling exceeds the bending strength of the ice plate. This mechanism leads to the formation of circumferential cracks in the ice (Michel and Blanchet, 1983) and is referred to in this paper as buckling failure. Buckling failure occurs for high aspect ratios and can develop at both high and low velocities of ice. When buckling failure at high velocities occurs after a period of ice crushing against the structure we refer to it as failure in mixed crushing and buckling.

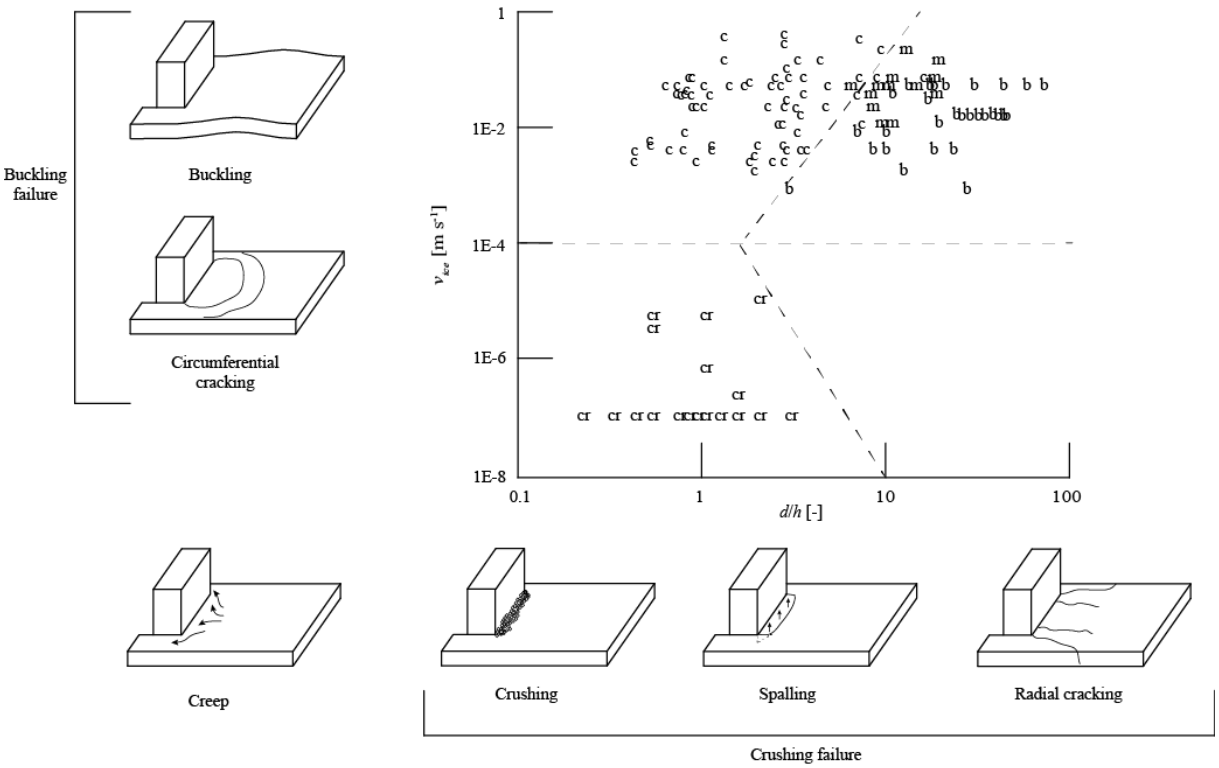

Figure 1 – Failure mode map for model-scale conditions based on the data reported by Timco (1991). Dashed lines indicate transitions between different failure modes. Sketches of distinct types of failure and fracture are shown. Legend: cr – creep, c – crushing failure (crushing, crushing with spalling, and crushing with radial cracking), b – buckling failure, m – mixed crushing and buckling failure.

The transitions between different failure modes are indicated in Figure 1 by dashed lines. A transition velocity can be identified which marks the change from creep to crushing, indicated by the horizontal dashed line. The transition velocity is expected to depend on ice properties similar to the ductile-to-brittle transition strain rate in compression of small ice-samples (Schulson and Duval, 2009). The global load on a structure is typically largest at or around the transition velocity for low aspect ratios for which the transition occurs from creep to crushing failure as, for example, can be observed in the results of experiments with rigid indenters by Sodhi and Morris (1984). For increasing velocity with respect to the transition velocity the ice load levels off to a more or less constant mean value at high velocities. A transition from creep to buckling failure and from crushing to buckling failure occurs for high aspect ratios or thin ice when the critical buckling load of the ice sheet is less than the maximum load due to crushing or creep. For such aspect ratios the maximum global load as a function of velocity no longer occurs at the transition velocity but at high velocities where mixed crushing and buckling failure is observed (Sodhi and Morris, 1984).

In the next section we present an integrated phenomenological model for simulation of creep, crushing failure, and buckling failure as defined above.

3. MODEL DESCRIPTION

In this section we introduce a phenomenological model for combined creep, crushing and buckling of level ice acting on a vertically-sided structure. An overview of the model is presented in Figure 2. The structure is modelled as a single-degree-of-freedom oscillator defined by its mass M_s [kg], damping C_s [kg s^{-1}], stiffness K_s [kg s^{-2}], displacement $u_s(t)$ [m], and structural width d_s [m]. This simple approximation is considered sufficient for the study in this paper, however a more detailed model of the structure can be straightforwardly implemented. The ice is assumed to have sufficient inertia such that its motion can be characterized by a constant indentation velocity v_{ice} [m s^{-1}]. The ice load on the structure $F_{ice}(t)$ [N] is the summation of the loads from N individual creep-crushing elements at the contact zone between ice and structure. Out of plane motion of the ice $w(x,t)$ [m] outside of the creep-crushing zone is modelled by a wedge beam on elastic foundation. In Section

3.1 and 3.2 the governing equations, conditions of failure, and definition of input parameters for the creep-crushing elements and the wedge beam on elastic foundation are introduced.

The model is studied numerically by application of a central difference scheme with respect to the spatial coordinate to discretize the ice beam into N_{beam} elements and rewriting the governing set of equations into a system of first order differential equations (state-space representation) which are solved in the time domain by application of the 4th order Runge-Kutta method. Event functions are implemented for the detection of contact, stick-slip behaviour of the creep-crushing elements, and failure of the ice by bending or crushing.

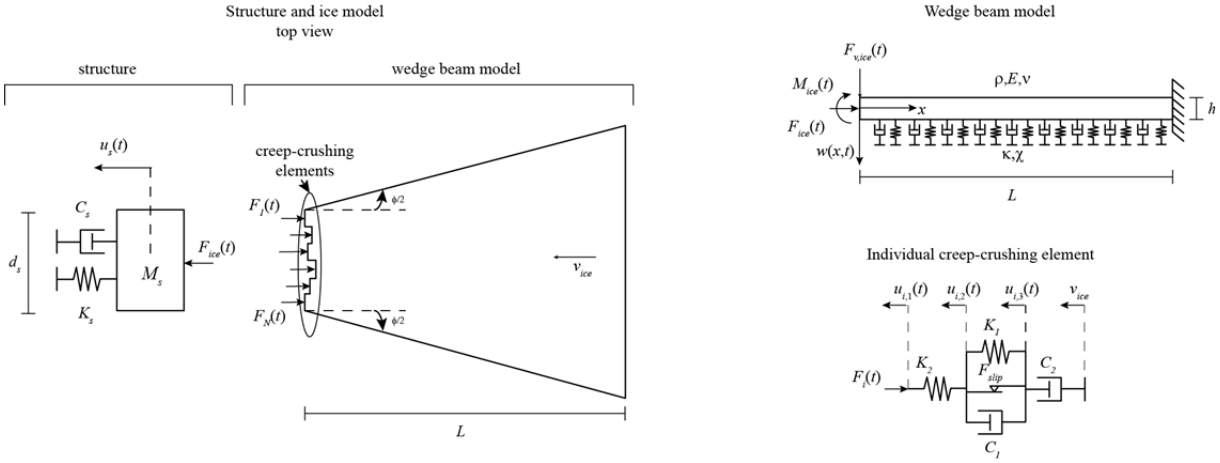

Figure 2 – Model for combined creep, crushing and buckling of ice acting on a vertically sided offshore structure. The structure is modelled as a single-degree-of-freedom oscillator. The ice model consists of a wedge beam on elastic foundation to model the flexural motion and *N* individual creep-crushing elements at the ice-structure interface to model the in-plane deformation and failure of the ice in the contact area.

3.1. Creep-crushing elements

Creep and crushing is taken into account by considering N creep-crushing elements as shown in Figure 2 for which the behaviour in terms of crushing is described in detail in Hendrikse and Metrikine (2015). The elements represent the area of contact between the structure and intact ice, where it is assumed that the load from broken ice pieces in contact with the structure is small and can be neglected. In this paper we have added a dashpot with coefficient C_2 [kg s^{-1}] to each individual element in order to model creep of ice at low rates in a simplified manner. It is not attempted to model primary, secondary, and tertiary creep deformation in detail, but to allow for the elements in the model not to fail at low velocities which is then defined as creep in the model. Creep of ice occurs below a transition velocity defined as v_{trans} [m s^{-1}] as illustrated in Figure 1 and discussed in Section 2. We assume the transition velocity not to vary with changes in d_s and h in which case the dashpot coefficient C_2 can be determined from the condition that no creep-crushing element should fail for indentation velocities below v_{trans}. An element shown in Figure 2 is set to fail when the deformation in the spring with stiffness K_2 [kg s^{-2}] exceeds a critical deformation δ_{crit} [m]:

$$u_{i,2}(t) - u_{i,1}(t) = \delta_{crit} \tag{1}$$

which yields for the dashpot coefficient C_2:

$$C_2 = \frac{K_2 \delta_{crit}}{v_{trans}} \tag{2}$$

For each element the initial position is drawn from a uniform distribution $\mathrm{U}(0, r_{\max})$ where $r_{\max}$ [m] is the maximum offset of an element after failure. The equations of motion for a single element are given by:

$$u_{i,1}(t)=\begin{cases}u_{i,2}(t) & no\ contact\\ u_s(t) & contact\end{cases}$$

$$\dot{u}_{i,2}(t)=\begin{cases} v_{ice} & no\ contact\\ \frac{K_2}{C_2}\left(u_s(t)-u_{i,2}(t)\right)+v_{ice} & contact\ stick\\ \frac{K_2}{C_1}\left(u_s(t)-u_{i,2}(t)\right)+\frac{K_1}{C_1}\left(u_{i,3}(t)-u_{i,2}(t)\right)+\frac{K_2}{C_2}\left(u_s(t)-u_{i,2}(t)\right)+v_{ice}+\frac{F_{slip}}{C_1} & contact\ slip\end{cases} \quad (3)$$

$$\dot{u}_{i,3}(t)=\begin{cases} v_{ice} & no\ contact\\ \frac{K_2}{C_2}\left(u_s(t)-u_{i,2}(t)\right)+v_{ice} & contact\end{cases}$$

where $u_{i,1}$ [m], $u_{i,2}$ [m], and $u_{i,3}$ [m] are displacements of characteristic points of element i as illustrated in Figure 2, K_1 [kg s^{-2}] is the stiffness of the centre spring of the element and C_1 [kg s^{-1}] is the damping coefficient of the centre dashpot of the element which define the visco-plastic deformation of the ice at low loading rates in the model, and F_{slip} [N] is the activation force of the sliding element (maximum force that it can hold at stick). Situations of no contact, contact where the sliding element sticks, and contact where the sliding element slides are distinguished.

The creep-crushing model has eight input parameters namely: $K_2, C_2, K_1, C_1, r_{\max}, N, \delta_{crit}, F_{slip}$. For now we cannot define these parameters purely based on physical ice properties as the required experimental data is not available. Therefore a method of defining the input parameters has been developed which relies on existing measurement data, hereafter referred to as reference measurements. The model can be used to simulate different scenarios under the assumption that the deformation and fracture behaviour of ice can be described by its micro-properties and that the effect of changes in structural properties and ice thickness only affect the behaviour as a result of the interaction between ice and structure. The limitation of this approach being that the model can only be applied for ice conditions for which reference measurements are available.

The eight input parameters can be defined based on eight reference measurements obtained from a scenario where an ice sheet of thickness h_{ref} [m] acts on a rigid structure of width d_{ref} [m] and low aspect ratio d_{ref}/h_{ref} such that no buckling occurs. The eight reference measurements are illustrated in Figure 3. We assume that the mean global ice load and standard deviation of the global ice load in crushing at high velocities level off to a constant value based on the experimental results presented by Sodhi (1998). These two values $F_{ref,mean}$ [N] and $F_{ref,std}$ [N] are the first two reference measurements. The value for the transition velocity which marks the transition between creep and crushing $v_{ref,trans}$ [m s^{-1}] is the third reference measurement. It is assumed that for this velocity the highest maximum global ice load can develop on a rigid structure which is $F_{ref,max}$ [N]. In order to define the trend in mean global load one additional measurement point is needed for a velocity close to the transition velocity in order to capture the slope of the curve. For this the mean global ice load at a velocity of twice the transition velocity is chosen $F_{ref,mean,2}$ [N]. Local deformation of the ice is defined based on a reference measurement for the time moment $t_{ref,peak}$ [s] at which the global peak load occurs at the transition velocity, and a value for the frequency in the spectrum of the global ice load which contains the major part of the energy $f_{ref,peak}$ [s^{-1}] at a high indentation velocity $v_{ref,high}$ [m s^{-1}]. The last reference measurement is the fraction of critical deformation upon which the ice behaves purely elastic c_{ref} [-]. The latter is not shown in Figure 3, but links directly to observations on first crack formation in compression of ice. The ice behaviour in the model is elastic up to a fraction c of the critical deformation of an individual element upon which sliding occurs and visco-plastic deformations of the ice can develop when the sliding force is defined as $F_{slip}=cK_2\delta_{crit}$. The parameter c is directly defined by c_{ref} in this case.

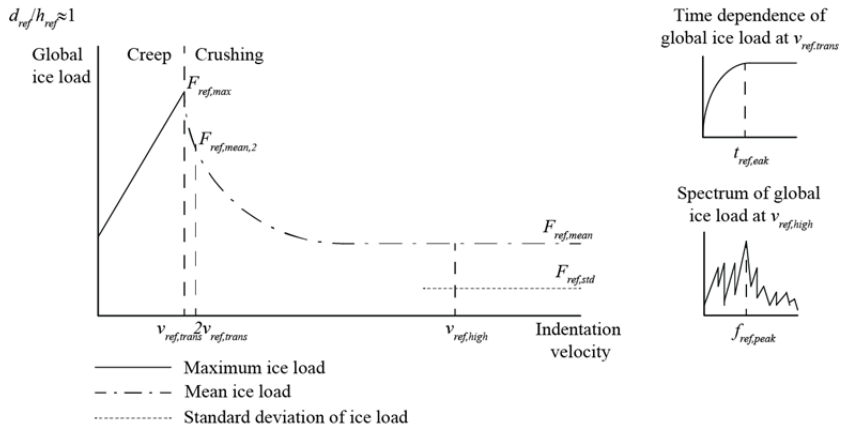

Figure 3. Example illustration of input curve used to define the parameters of the creep-crushing elements in the model. The curve should be obtained from measurements with rigid indenters for the specific ice conditions investigated.

The input parameters of the phenomenological model can be chosen such that the model reproduces the behaviour as defined by the reference measurements and illustrated in Figure 3. In order to define the relations between the input parameters and the reference measurements equations for the mean global load, standard deviation of the global load, and peak frequency in the spectrum of the global load in the model are defined:

$$F_{mean}\left(v_{ice}\right) = N\frac{K_2\int_0^{t_{fail}} u_{i,2}dt}{\frac{E(r)}{v_{ice}}+t_{fail}}$$

$$F_{std}\left(v_{ice}\right) = \sqrt{N\left(\frac{K_2^2\int_0^{t_{fail}} u_{i,2}^2dt}{\frac{E(r)}{v_{ice}}+t_{fail}}\right)-F_{mean}^2} \qquad (4)$$

$$f_{peak}\left(v_{ice}\right) = \frac{E(r)+\delta_{crit}}{v_{ice}}$$

where t_{fail} [s] is the time moment at which an individual creep-crushing element fails against a rigid structure when the ice is moving at a velocity v_{ice} which can be obtained by solving the differential equation governing the motion of an ice element in the model, and E(r) is the expected value of the offset of an element after failure which is equal to $0.5r_{max}$ for the uniform distribution used. The assumption is made here that at high velocities the elements in the model behave almost elastically to determine the expected peak frequency. By using these equations and, additionally, the equation for the maximum load in the model:

$$F_{\max} = NK_2\delta_{crit} \qquad (5)$$

the input parameters $K_2, r_{\max}, N, \delta_{crit}$ can be expressed in terms of the reference measurements as:

$$\delta_{crit} = 2\frac{F_{ref,mean}}{F_{ref,\max}}\frac{v_{ref,high}}{f_{ref,peak}}$$

$$r_{\max} = \frac{2v_{ref,high}}{f_{ref,peak}} - 2\delta_{crit}$$

$$N_{ref} = \frac{\frac{2}{3}F_{ref,\max}F_{ref,mean} - F_{ref,mean}^2}{F_{ref,std}^2} \qquad (6)$$

$$K_2 = \frac{hF_{ref,\max}}{h_{ref}N_{ref}\delta_{crit}}$$

where the simplification is made that at high velocities the creep-crushing elements behave elastically and the deformation $u_{i,2}$(t) is approximately given by $v_{ice}t$. The value for K_2 is scaled with the ice thickness such that the

global load scales linearly with variations in ice thickness in the model. N_{ref} is the amount of elements which is needed to reproduce the statistics of the global ice load for a structure with reference width d_{ref}. To incorporate the dependence of global load on structure width the number of elements N in the model is defined as:

$$N = \frac{d_s}{d_{ref}} N_{ref} \qquad (7)$$

This results in a linear dependence of the maximum and mean global ice load on structure width, and a decrease of the standard deviation of the global ice load with increasing structure width. The final two input parameters of the model K_1 and C_1 have to be determined by solving two additional equations to match the remaining two reference measurements $F_{ref,mean,2}$ and $t_{ref,peak}$:

$$\begin{aligned} F_{ref,mean,2} &= N_{ref} \frac{K_2 \int_0^{t_{fail}} u_{i,2}\left(t, 2v_{ref,trans}\right) dt}{\frac{E(r)}{2v_{ref,trans}} + t_{fail}} \\ t_{ref,peak} &= \frac{E(r)}{v_{ref,trans}} + t_{f1} \\ u_{i,2}\left(t_{f1}, v_{ref,trans}\right) &= f_1 \delta_{crit} \end{aligned} \qquad (8)$$

The time moment at which the peak load occurs in the model at a velocity $v_{ref,trans}$ is equal to infinity. An approximation is therefore made setting the time moment of peak load equal to $f_1\delta_{crit}$ [m].

3.2. Flexural behaviour of the ice

Flexural behaviour of the ice is included by considering a wedge beam on elastic foundation as shown in Figure 2. The equation of motion of the beam is given by:

$$\begin{aligned} & Dw(x,t)'''' + 2\frac{D}{d(x)} d(x)' w(x,t)''' + \frac{F_{ice}(t)}{d(x)} w(x,t)'' + \kappa w(x,t) + \chi \dot{w}(x,t) + \rho h \ddot{w}(x,t) = 0 \\ & d(x) = d_s + (L-x) 2\tan\left(\frac{\phi}{2}\right) \\ & D = \frac{Eh^3}{12\left(1-\nu^2\right)} \end{aligned} \qquad (9)$$

where primes indicate spatial derivatives with respect to x, over dots represent derivatives with respect to time, L is the beam length [m], h the ice thickness [m], ϕ the wedge angle [rad], κ the specific weight of water [kg m^{-2} s^{-2}], ρ the mass density of ice [kg m^{-3}], E the Young's modulus of ice [N m^{-2}], ν the Poison ratio of ice [-], and χ a distributed viscous damping per unit area [kg m^{-2} s^{-1}]. The beam is considered fixed at a distance L away from the structure and subject to axial force $F_{ice}(t)$, bending moment $M_{ice}(t)$ [Nm], and vertical force $F_{v;ice}(t)$ [N] at the ice-structure interface defined in terms of boundary conditions as:

$$\begin{aligned} & w(L,t) = w(x,t)'\big|_{x=L} = 0 \\ & -Dd(x) w(x,t)''\big|_{x=0} = M_{ice}(t) = \mathrm{U}(0, 0.001) F_{ice}(t) \\ & -Dd(x) w(x,t)'''\big|_{x=0} - Dd(x)' w(x,t)''\big|_{x=0} + F_{ice}(t) w(x,t)'\big|_{x=0} = F_{v;ice}(t) = -\mathrm{sgn}\left(\dot{w}(x,t)\big|_{x=0}\right) \mu F_{ice}(t) \end{aligned} \qquad (10)$$

where the bending moment M_{ice} is introduced to cause a disturbance of the in-plane equilibrium of the beam such

as to allow buckling to develop. The value is chosen small such that if failure by exceedance of the flexural strength occurs this is a result of buckling instability and not of pure bending of the beam. Upon failure of a creep-crushing element a new value for the eccentricity is drawn from a uniform distribution $\mathrm{U}(0, 0.001)$. The vertical force $F_{v;ice}$ is implemented to include frictional sliding in vertical direction along the ice-structure interface characterized by friction coefficient μ [-].

Failure is set to occur when the bending stress at one cross-section in the beam, x^*, exceeds the flexural strength at a certain moment in time:

$$\left| \frac{6D}{h^2} w(x,t)''\big|_{x=x^*} \right| - \frac{F_{ice}(t)}{hd(x^*)} = \sigma_f \tag{11}$$

where σ_f [N m^{-2}] is the flexural strength of the ice. Upon failure the ice beam is removed from the model until the distance over which the ice has broken has been covered and new contact between the ice and structure is established.

4. MODEL APPLICATION FOR ICE ACTION ON RIGID STRUCTURES

In this section we discuss predictions of the model for the case of a model-ice sheet acting against a rigid vertically-sided structure. The results demonstrate the applicability of the model for modelling creep, crushing, and buckling of ice. Input parameters of the model are shown in Table 1. The model-scale ice properties are based upon the values for urea ice reported by Sodhi and Morris (1984). In their report results of indentation experiments are shown which contain a large portion of the required reference measurements.

With respect to the creep-crushing elements the values for $F_{ref,max}$, $F_{ref,mean}$, $F_{ref,std}$, $v_{ref,high}$, and $f_{ref,peak}$ for the defined d_{ref} and h_{ref} can be obtained from tables in the appendix of the report by Sodhi and Morris (1984), from which we have averaged the observations from the tests at 25 February 1983 and 3 February 1983. For the transition velocity $v_{ref,trans}$ an estimate is made of 1 mm s^{-1} which is a bit higher than the reported values for small-grained freshwater ice by Nakazawa and Sodhi (1990). The value for $t_{ref,peak}$ is also estimated based on that report taking into account that the model assumes a rough ice edge at the start and the experiments were carried out with a prepared flat surface of the ice. The value for $F_{ref,mean,2}$ is estimated based on the ratio between the mean contact area during high velocity crushing and close to the transition from creep to crushing in the experiments by Takeuchi et al. (2001).

For the wedge beam model the values for E, and σ_f are obtained from Sodhi and Morris (1984). The length of the beam is chosen to be much larger than the ice thickness and set at 9 m and a wedge angle of 45^o is chosen based on Kerr (1978). Values for the Poison ratio and mass density of Urea ice are based on the work by Timco (1980). The distributed spring stiffness is defined by the specific weight of water, and the distributed viscous damping is chosen such that energy reflected from the fixed boundary of the ice beam is limited. The dynamic friction coefficient is chosen based upon reference values for kinetic friction between ice and steel.

The reference measurements used here to define the input of the model are chosen with care to obtain ice behaviour in the model which matches model-scale observations. Validation of the proposed method of defining input parameters requires experimental effort and the results from simulations presented hereafter will change when different input parameters are defined. However, as long as the general ice load dependence as sketched in Figure 3 is assumed to reflect the trend in ice loads on a rigid structure, changes in parameters will mainly affect the location of the boundaries between creep and crushing, and between the different regimes of ice-induced vibrations when flexible structures are considered in the model. For the wedge beam approach the same is valid. The competition between buckling and crushing remains in the model unless the wedge angle is chosen as 0 degrees, which results in a straight beam for which the ice will either always crush or always buckle.

Table 1 - Input parameters for model-scale urea ice based on values reported in Sodhi and Morris (1984).

Parameter:	Input value:	Dimension:
d_{ref}	0.05	[m]
h_{ref}	0.055	[m]

$v_{ref,high}$	0.13	[m s^{-1}]
$v_{ref,trans}$	0.001	[m s^{-1}]
$F_{ref,max}$	5500	[N]
$F_{ref,std}$	500	[N]
$F_{ref,mean}$	1500	[N]
$f_{ref,peak}$	11	[Hz]
$F_{ref,mean,2}$	3750	[N]
$t_{ref,peak}$	150	[s]
c_{ref}	0.3	[-]
L	9	[m]
E	1.74 10^{8}	[N m^{-2}]
υ	0.33	[-]
κ	10055	[kg m^{-2} s^{-2}]
ϕ	0.5π	[rad]
χ	512.5	[kg m^{-2} s^{-1}]
ρ	950	[kg m^{-3}]
σ_f	170000	[N m^{-2}]
μ	0.03	[-]
N_{beam}	180	[-]

We generate a failure map for model-scale conditions by varying the indentation velocity v_{ice} between 0.0001 m s^{-1} and 1 m s^{-1} and the structural width d_s between 0.05 m and 1.7 m in the model. The result is shown in Figure 4. We distinguish between creep, crushing, buckling and mixed crushing and buckling failure. Each simulation is run for 10 seconds of the simulated signal, or an indentation distance of 30 failure lengths δ_{crit}, whichever greater. Creep is defined to occur when during the simulation no creep-crushing element fails and no buckling failure occurs. Buckling is defined to occur when the ice fails according to Eq. (11) before a single creep-crushing element has failed. In case only creep-crushing elements fail the failure mode is set to be crushing, whereas a combination of crushing and buckling failure is defined as mixed mode failure.

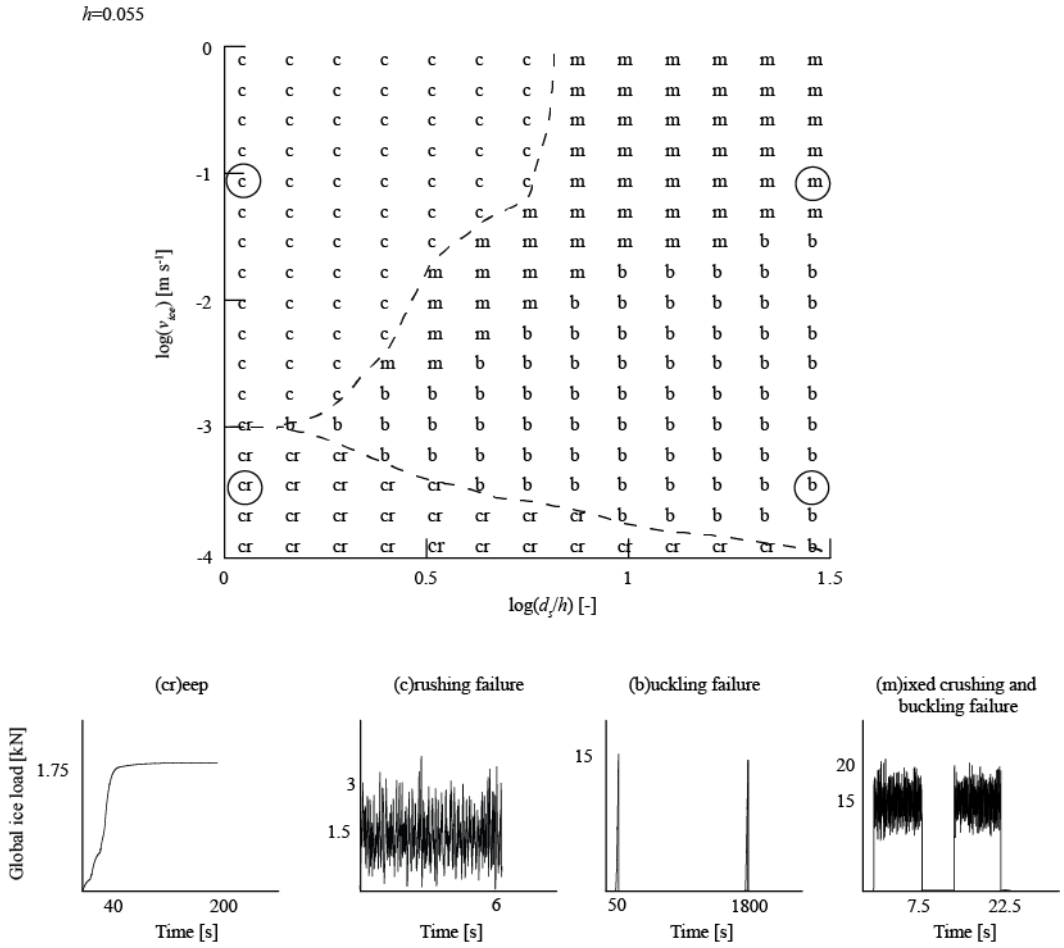

Figure 4 – Top: Numerically generated failure map for representative urea ice conditions given in Table 1 based on ice properties reported in Sodhi and Morris (1984). Bottom: Ice load signals generated with the model for the different types of failure at conditions circled in the failure map are shown at the bottom. Legend: cr – creep, c – crushing failure, b – buckling failure, m – mixed crushing and buckling failure.

Comparing the obtained failure map in Figure 4 with the one based upon experimental observations shown in Figure 1 one can see that the trends are reproduced by the model. For indentation velocities below v_{trans} the model predicts either creep or buckling failure to occur depending on the aspect ratio. Crushing occurs for velocities above v_{trans} and a transition to mixed failure or buckling takes place for an aspect ratio between 2 and 10 approximately, depending on the indentation velocity v_{ice}.

Typical time dependencies of the ice load as predicted by the model for each of the failure modes are also shown in Figure 4 and can be compared with the signals given by Timco (1987). Creep shows the load levelling off after some time of loading as all creep-crushing elements come into contact with the structure. Crushing shows a typical random load signal around a mean value. Buckling is characterized by a load build-up phase, followed by a load drop to zero resulting from global failure. Mixed mode failure shows some time of crushing until buckling failure occurs. The time of crushing in this case is governed by the time needed for the ice to reach an out-of-plane deformed state which causes global failure.

The dependence of the maximum global load on velocity for an aspect ratio of one and thirty is shown in Figure 5. The ice loads in this figure are scaled with respect to the mean load for crushing at high velocities. The model reproduces the typical trend in the dependence of the global load on indentation velocity in case of creep and crushing at an aspect ratio of one. The maximum ice load is observed around the transition velocity above which the load decreases towards a more or less steady value for increasing velocity. The disappearance of this trend for higher aspect ratios as observed in model-scale experiments (Sodhi and Morris, 1984) is also reproduced as shown for an aspect ratio of thirty. The trend of reducing maximum global load from the transition velocity is no longer observed at such high aspect ratio. The latter is a result of buckling failure.

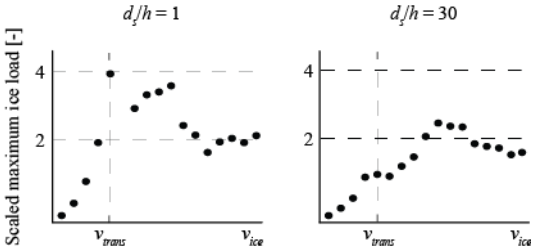

Figure 5 – Dependence of maximum global ice load on indentation velocity for an aspect ratio of one and thirty. The maximum global load is scaled with respect to the mean load for crushing at high velocities.

The transition between creep and buckling, or crushing and buckling in the model is governed by the ratio between the global crushing load and the critical buckling load of the wedge beam. This ratio can be approximated by:

$$\frac{F_{crush}\left(v_{ice}\right)\dfrac{hd_s}{h_{ref}d_{ref}}}{P} = 1 \tag{12}$$

where $F_{crush}\left(v_{ice}\right)$ [N] is the dependence of the global load on indentation velocity for the reference case as defined in Figure 3, and P [N] is the critical buckling load of the wedge beam. In order to gain some insight in the dependence of the critical buckling load in the model on the different input parameters we determined the static critical buckling load based upon Eq. (9) and (10) by solving the generalized eigenvalue problem applying the finite difference method. This particular analysis does not include the creep-crushing elements at the boundary between ice and structure, as opposed to the other results presented in this paper. The result in terms of the three dimensionless parameters governing the problem is shown in Figure 6. The result presented here is valid only for boundary conditions defined by Eq. (10) where we did not consider the external bending moment M_{ice}. For different boundary conditions similar maps can be straightforwardly reproduced. An analytical solution for buckling of a semi-infinite wedge can be found in Nevel (1980).

Figure 6 shows that the critical buckling load P does not increase proportionally with an increase in structural width d_s, whereas the global load due to creep and crushing increases proportionally with d_s as given by Eq. (12). As a result a transition from crushing to buckling occurs for large structural width d_s provided that all other parameters are kept constant. As the crushing load depends on velocity the transition does not occur at a single value of d_s for all indentation velocities, as can be observed from the failure map in Figure 4. The actual value of d_s for which the transition occurs increases with increasing κ, D, ϕ^*, and h and decreases for increasing $F_{crush}\left(v_{ice}\right)$, where ϕ^* is defined by:

$$\phi^* = 2\tan\left(\phi/2\right) \tag{13}$$

The length of the beam has only a small effect on the results as buckling occurs near the ice-structure interface, but should not be too short in relation to the structure width and ice thickness.

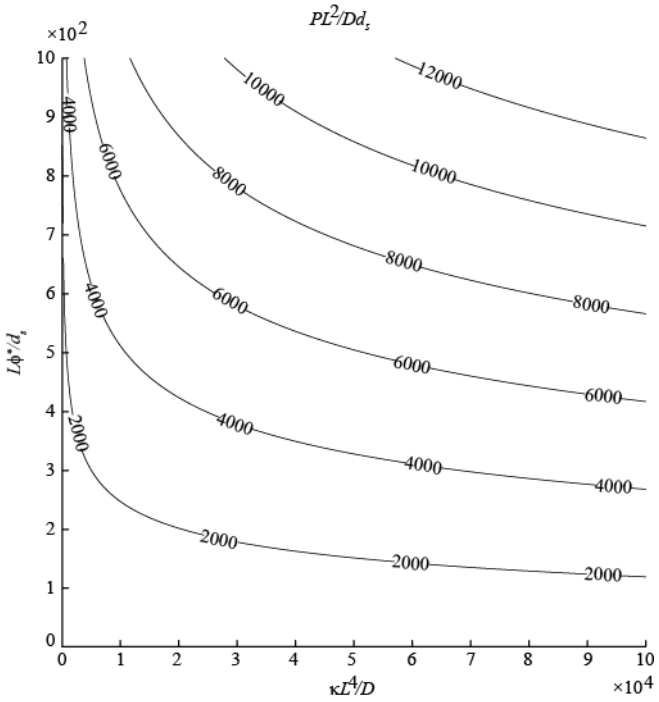

Figure 6 – Critical buckling load of a wedge beam on elastic foundation in a fixed-free configuration defined by Equation (9) and (10).

The results obtained with the model for the case of level ice action on a rigid vertically-sided structure shown in this section illustrate that the model qualitatively captures the different failure modes of ice which may occur, and generates representative load signals and trends in statistical properties of the ice load. In the next section the model is applied to study the development of ice-induced vibrations in cases associated with ice failure by mixed crushing and buckling.

5. ICE INDUCED VIBRATIONS AND ICE BUCKLING

In this section we present the results of a study into the development of ice-induced vibrations in cases associated with ice failure by mixed crushing and buckling. All simulations are performed with ice defined by the properties given in Table 1. In Section 5.1. we show the development of ice-induced vibrations for a structure with various widths of which the dynamic properties are scaled with respect to the ice load. Results obtained with this configuration illustrate the effect of changes in the failure mode of ice on the development of ice-induced vibrations and the effect of flexibility of the structure on the occurring failure mode. In Section 5.2. we discuss one particular case for which the flexibility of the structure results in intermittent crushing that prevents buckling failure from occurring under the conditions that lead to buckling for indentation on a rigid structure. In Section 5.3. we show the development of ice-induced vibrations for a structure with fixed properties for different values of ice thickness. This is a general case which is applicable for real structures which encounter varying ice conditions over their lifetime. Obtained results are further discussed in Section 6.

5.1. A structure with scaled dynamic properties

In this section we simulate a flexible structure with low damping in ice conditions defined by the parameters given in Table 1, for which the occurring failure mode of ice as a function of structure width and velocity is shown in the failure map in Figure 4. The structural properties are chosen arbitrarily such that for an aspect ratio of one intermittent crushing and frequency lock-in occur over a range of velocities. We defined a natural frequency of 2.5 Hz, damping ratio of 3% of critical, and structural stiffness:

$$K_s = 0.5 K_2 N_{ref} \frac{d_s}{d_{ref}} \quad (14)$$

This choice of the structural properties assures that the dynamic interaction scales with changing width of the structure. The results obtained thereby elucidate the effect of mixed crushing and buckling failure on the development of ice-induced vibrations and the effect of flexibility of the structure on the observed failure mode.

With respect to the results for ice-induced vibrations obtained with the model we distinguish between intermittent crushing, frequency lock-in, and continuous brittle crushing. Intermittent crushing is said to occur in the model if a quasi-periodic saw-tooth pattern with a period greater than the natural period of the structure is observed in the time dependence of both the ice load and structural displacement. Frequency lock-in is defined to occur in the model, based on observations by Toyama et al. (1983), in the case when a periodic motion of the structure occurs with a period close to its natural period (observed in the absence of the ice loading) and with the maximum velocity equal to or slightly higher than the indentation velocity.

Figure 7 shows the occurring types of ice-induced vibrations in the plane of velocity and width of the structure. For an aspect ratio of one, intermittent crushing (icr) is predicted at velocities between 0.001 m s^{-1} and 0.025 m s^{-1} approximately. From 0.025 m s^{-1} up to 0.075 m s^{-1} frequency lock-in (fli) is predicted and above 0.075 m s^{-1} brittle crushing (cbr) is observed corresponding to a random response of the structure. As we scaled the structural properties with the increasing ice load following Eq. (14) the range of velocities for which ice-induced vibrations occur does not vary with changing width of the structure unless buckling failure occurs, limiting the development of ice-induced vibrations.

Ice-induced vibrations which develop for a limited interval of time followed by buckling are indicated with an asterisk. Such vibrations mainly develop for the failure conditions in which mixed mode failure would be expected based on the failure map shown in Figure 4. These cases sometimes include only one or two cycles of vibration before buckling failure occurs. When buckling occurs without crushing, or the duration of mixed mode failure is too short, ice-induced vibrations are no longer observed.

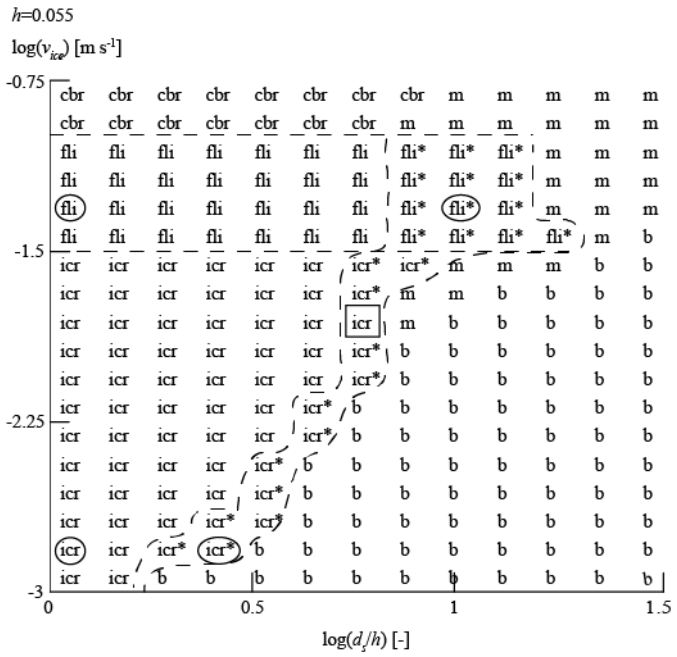

Figure 7 – Predicted types of ice-induced vibrations for a structure whose dynamic properties are scaled according to Equation (14). Time dependencies of displacement of the structure and ice load of the circled cases are shown in Figure 8. The case indicated by the rectangle is discussed in more detail in Section 5.2. Legend: icr – intermittent crushing, fli – frequency lock-in, cbr - continuous brittle crushing, b – buckling, m – mixed crushing and buckling failure, icr* intermittent crushing followed by buckling failure, fli* frequency lock-in followed by buckling failure.

Examples of time-dependencies corresponding to intermittent crushing and frequency lock-in during crushing and mixed failure circled in Figure 7 are shown in Figure 8. With respect to intermittent crushing at a velocity of 0.002 m s^{-1} the results show that the maximum displacement and saw-tooth period are not affected by the flexural motion of the beam, whereas the vibrations are limited in duration for the higher aspect ratio due to buckling failure. For frequency lock-in at a velocity of 0.04 m s^{-1} oscillations of the structure are similar at low

and high aspect ratios, although also in this case the number of cycles is limited by the occurrence of buckling failure. Effects of upward and downward motion of the ice sheet on the crushing process are not included in the model and are to our knowledge not available from literature, but we expect these to be small given that crushing is a very local process. The results show that the development of ice-induced vibrations in cases of mixed buckling and crushing is primarily dependent on the ratio between the time required for buckling to result in failure, the buckling period, and the period of intermittent crushing or frequency lock-in.

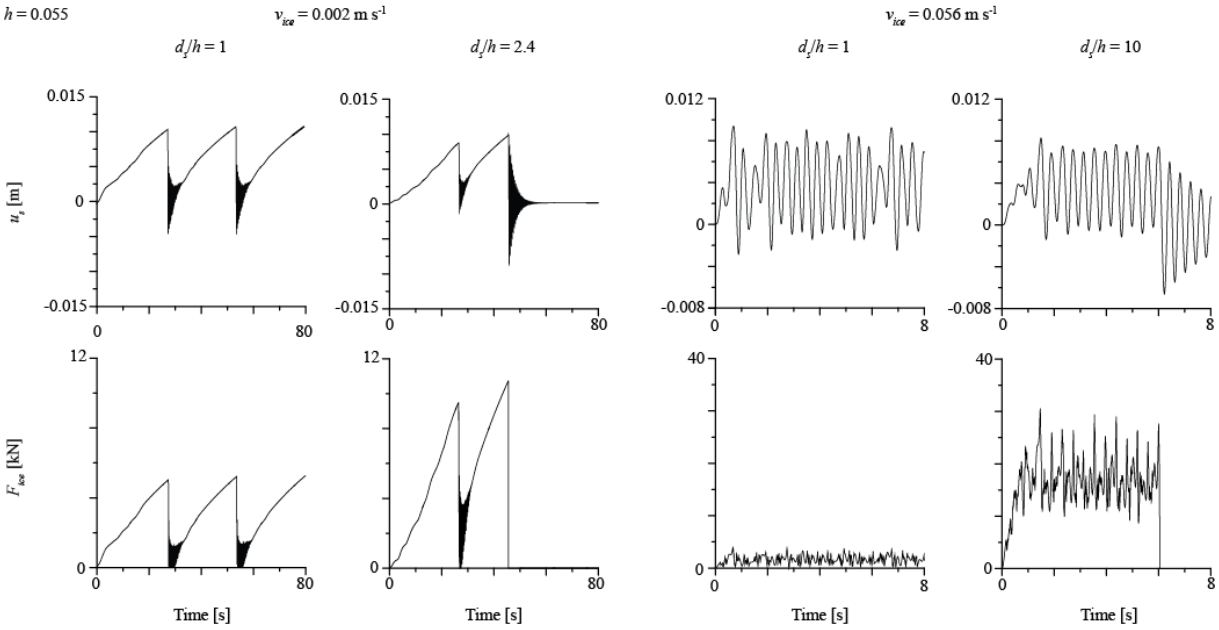

Figure 8 – Examples of structural displacement and global ice load during intermittent crushing and frequency lock-in in conditions of continuous crushing at an aspect ratio of 1, and mixed crushing and buckling failure at aspect ratios of 2.4 and 10, respectively. The conditions for which the signals are obtained are circled in Figure 7.

Figure 9 shows this buckling period as a function of velocity and width of the structure for indentation on a rigid structure as used to obtain the failure map in Figure 4. The buckling period shows a general decreasing trend for increasing velocity and increasing width. A limit value is reached for high velocity indentation. This is a result of the axial load no longer decreasing with increasing velocity as illustrated in Figure 3, and the load build-up time becoming shorter such that its contribution to the buckling period diminishes. An interesting region is obtained for aspect ratios between 3 and 30 roughly where with increasing velocity from the transition velocity the buckling period first reduces and then slightly increases again. This effect is caused by the dependence of the axial load on indentation velocity in relation to the critical buckling load as described in Section 4. Additionally, the frictional sliding at the ice-structure interface and randomness in the model have a large effect on the obtained buckling period for cases where the global ice load is close to the critical buckling load. Due to these effects it is difficult to predict the actual buckling period and the possibility for ice-induced vibrations to develop without simulating the interaction.

One effect which is observed is that the introduction of a flexible structure can cause the buckling period to increase with respect to the values shown in Figure 9. This happens mostly for cases in which intermittent crushing develops such as shown in Figure 8 for an aspect ratio of 2.4. During intermittent crushing the global ice load generally increases to a higher value than would be observed for the same conditions with a rigid structure. This might lead to the expectation that buckling would occur sooner. However, the large load drops which occur during intermittent crushing can result in the build-up of the out-of-plane deformation of the ice, ultimately causing the buckling failure, to diminish in between saw-tooth events thereby causing the buckling failure to be delayed, or not occur at all. In the next section we further illustrate this effect based on a simulation for which we found buckling failure to be prevented by continuous intermittent crushing.

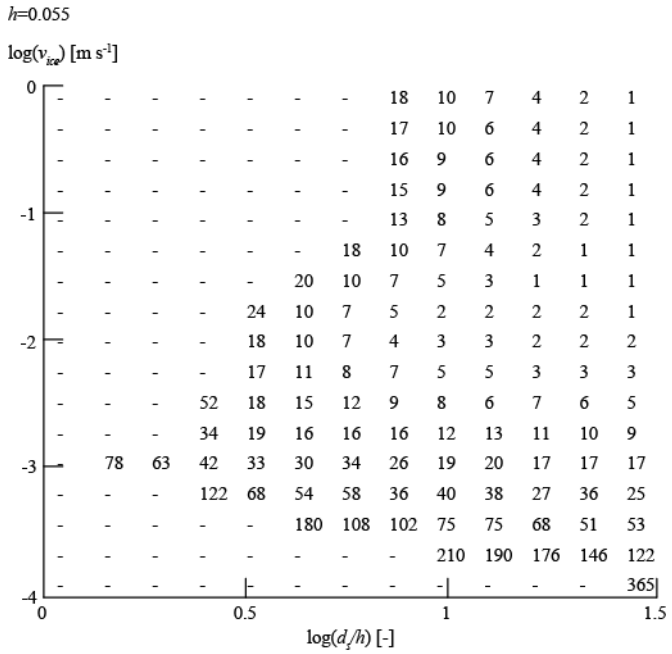

Figure 9 – Buckling period [s] for modelled ice as a function of indentation velocity and width of the structure. The period shows a general trend of decrease with increasing structural width and ice velocity.

5.2. Intermittent crushing limiting the development of buckling failure

In this section we show how ice-induced vibrations may prevent buckling failure from occurring instead of buckling failure limiting the duration of ice-induced vibrations. A case clearly illustrating the effect of structural motion on the development of buckling failure is indicated by the rectangle in Figure 7. For this case we expect the ice to fail in mixed crushing and buckling when looking at the failure map in Figure 4. The buckling period is expected to be approximately 7 seconds as shown in Figure 9. However, as illustrated in Figure 10, sustained intermittent crushing occurs for at least 16 seconds, the duration of the particular simulation. The vertical displacement of the front of the wedge beam is also shown in Figure 10, which for the given boundary conditions is a representative measure of the bending of the beam. Comparing the displacement of the front of the beam for the case in which ice acts on a rigid structure with the indentation on a flexible structure shows the reason for the buckling failure to be prevented.

For the rigid structure the ice load builds up to, and then oscillates around, an average value which exceeds the buckling limit of the beam causing the beam to become unstable and deform until buckling failure occurs. For the flexible structure the ice load builds up to a higher level, far exceeding the critical buckling load, however before the beam can sufficiently deform to cause buckling failure the ice load drops to a close to zero value allowing the beam to return to its equilibrium position. In such particular case of the intermittent crushing period being smaller than the buckling period the development of ice-induced vibrations thus prevents buckling failure from happening.

The result shown in Figure 10 is highly dependent on boundary conditions, which determine how fast the beam can move back to the equilibrium position and on the randomness in the ice properties taken into account. Theoretically a similar result could be obtained for frequency lock-in as the ice load also oscillates periodically, and could oscillate around the critical buckling load, however we did not observe this in any of the simulations.

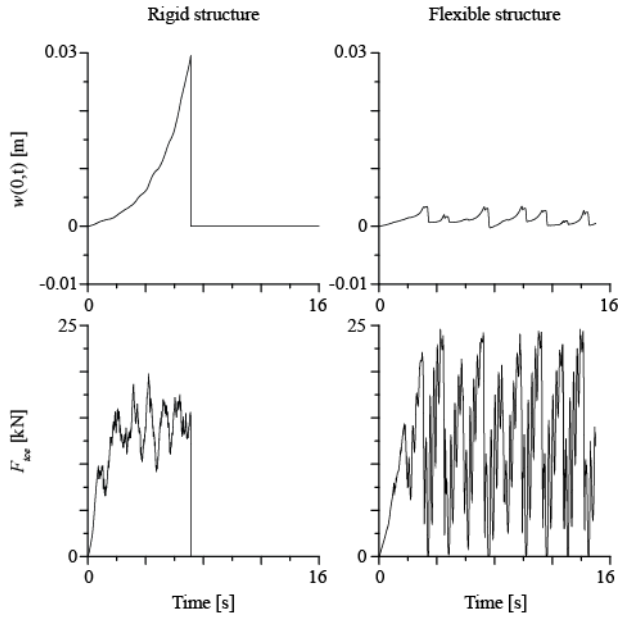

Figure 10 – Vertical displacement of the ice edge in contact with the structure and global ice load for a velocity of 0.018 $\mathrm{m\ s^{-1}}$**, aspect ratio of 5.6 and ice thickness of 0.055 m. Left: a rigid structure showing buckling failure to occur after 7 seconds of crushing. Right: Intermittent crushing on a flexible structure preventing the buckling failure.**

5.3. A structure in conditions of different ice thickness

We now consider a structure with fixed properties in conditions of different ice thickness. This situation resembles an offshore structure which encounters varying ice conditions over its lifetime, however we ran the situation for the model-scale ice properties given in Table 1. The structural properties are fixed to the following values: structural width of 0.25 m, natural frequency of 2.5 Hz, damping ratio of 3%, and structural stiffness of $2.5K_2N_{ref}$, with K_2 fixed for an ice thickness of 0.025 m. The ice thickness is varied from 0.025 m up to 0.25 m resulting in an aspect ratio varying between one and ten. Results of the simulation are shown in Figure 11 including a failure map generated with a rigid structure of 0.25 m width for the same ice conditions. Note that the vertical axis differs between plots as for ice-induced vibrations we did not simulate the range of velocities below the transition velocity. Nor the highest velocities were simulated for which continuous brittle crushing occurs.

The maximum velocity for which intermittent crushing and frequency lock-in occur generally decreases with decreasing ice thickness as a result of reduction of the global ice load. This can result in two situations when it comes to ice-induced vibrations in mixed failure conditions. First, the ice thickness for which mixed failure conditions occur might yield a too low global load level for ice-induced vibrations to develop. In this case there is no influence of buckling on the development of ice-induced vibrations or vice versa. The second case is that for which the global ice load is still large enough to cause ice-induced vibrations. In this case the criteria and conditions are the same as those discussed in the previous subsections. An analysis which considers pure crushing over the whole range of ice thicknesses would provide an upper bound for the aspect ratio for which ice-induced vibrations may develop for a given structure. If this upper bound aspect ratio is higher than the aspect ratio for which mixed failure is expected an integrated analysis taking into account all failure modes might give more realistic load signals for the design of such structure, provided that the model used for simulation of the ice load is validated to predict realistic ice load signals.

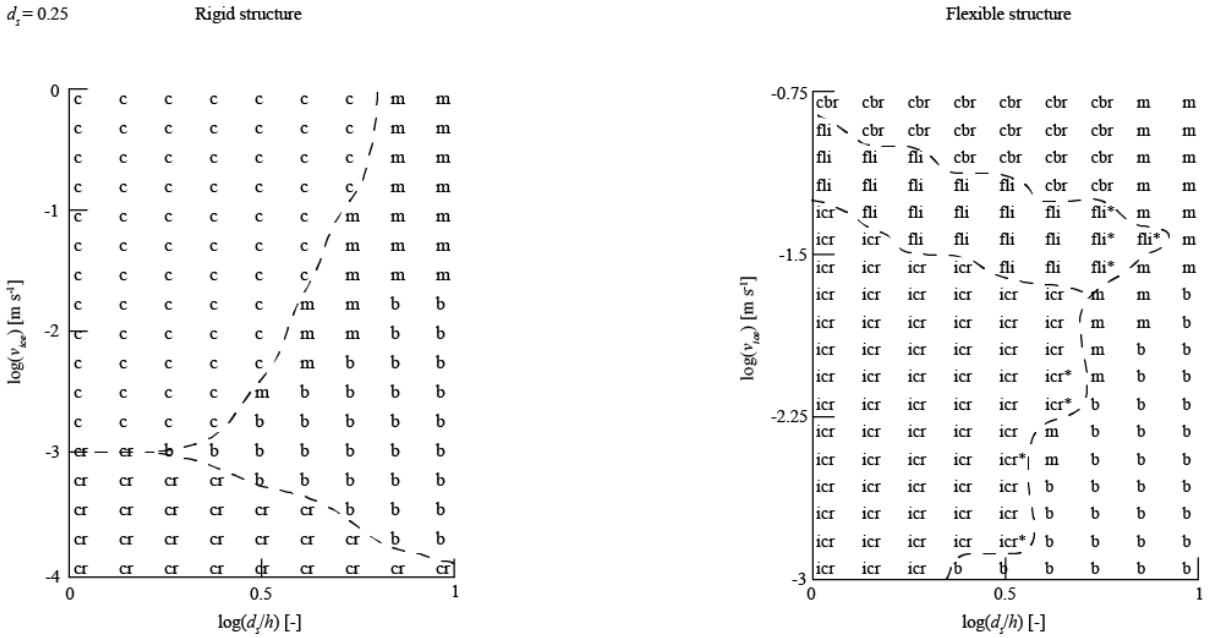

Figure 11 – Left: failure map for rigid structure of 0.25 m width for different values of ice thickness and velocity. Right: Occurrence of ice-induced vibrations for a flexible structure with a width of 0.25 m, 2.5 Hz natural frequency, and 3% damping as a percentage of critical, for varying ice thickness and velocity. Legend: cr – creep, c – crushing failure, b – buckling failure, m – mixed crushing and buckling failure, icr – intermittent crushing, fli – frequency lock-in, cbr - continuous brittle crushing, icr* intermittent crushing followed by buckling failure, fli* frequency lock-in followed by buckling failure.

6. DISCUSSION

The results presented in Section 5 show that three conditions should be met in order for ice-induced vibrations to develop in situations when the ice fails in the regime of mixed crushing and buckling. First, the ice crushing load and critical buckling load should belong in the range that allows for the mixed crushing and buckling mode to occur. Second, the time required for buckling failure to develop, referred to as the buckling period in this paper, must be significantly greater than the period of frequency lock-in or period of intermittent crushing. And third, ice-induced vibrations must be admissible for the given structural and ice properties. We will now discuss each of these conditions, followed by a discussion on failure maps for thick ice.

The condition for ice to fail in mixed crushing and buckling is defined by ice properties, boundary conditions, structural size, and structural shape. Each of these, having an effect on the critical buckling load and crushing load level, thereby affect the transition condition given by Equation (12). For specific ice conditions the critical buckling load dependence on ice and structural properties can be assessed by developing a map as shown in Figure 6. Boundary conditions play a significant role as, for example, the presence of large piles of rubble on top and below the ice would increase the critical buckling load significantly and hence crushing might be expected for conditions in which level ice without rubble would experience buckling failure. This example has already been mentioned by Blanchet et al. (1988) in discussion of the observations made on the Molikpaq structure in the Beaufort Sea. With respect to structural shape the development of radial cracks plays a role as well as the orientation of the load with respect to the formed wedges. The difference between a rectangular structure and cylindrical structure is illustrated in Figure 12. For a cylindrical structure the wedges have a smaller angle, resulting in lower buckling resistance, however the load on each wedge is also reduced when compared to the rectangular structure of same width. Therefore the transition between crushing and mixed failure might occur at higher aspect ratios (Kerr, 1978). For large circumferential buckling failure the wedge beam approach is not applicable and plate theory is perhaps a better choice.

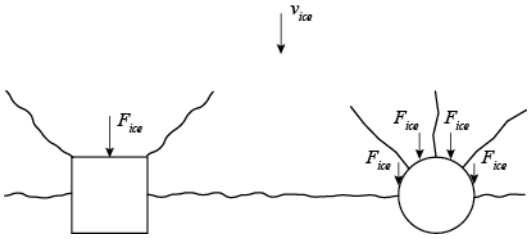

Figure 12 – Effect of the shape of the structure on development of radial cracks in the ice and global ice load distribution amongst different wedges of ice in contact with the structure.

The buckling period has been shown to depend on indentation velocity, aspect ratio and ice properties in general in Section 5. Further study is needed to quantify the dependence of the buckling period on these properties. Specifically, the applicability of the wedge beam model for quantitative modelling of this type of interaction needs to be considered first. We do however expect the observed trends to remain as the problem does not change significantly when more complex models for buckling are introduced as long as the buckling is considered in an elastic manner. The period of frequency lock-in, if it occurs, is well known to be around the natural frequency or slightly below the natural frequency of the structure. The period of saw-tooth oscillation during intermittent crushing is in general greater and decreases with increasing indentation velocity (Sodhi, 1991). No general rule of thumb is yet available to estimate those periods based on given ice properties, so one has to rely on numerical simulations to obtain an indication for those.

The question of whether or not ice-induced vibrations can develop for given structural properties and ice conditions is an entire field of study which has not matured enough to provide quantitative answers. General trends show that frequency lock-in cannot develop for high natural frequencies and in cases involving large damping. Ice velocity plays a role in terms of its proximity to the transitional velocity. With respect to intermittent crushing the stiffness of the structure as compared to the ice load level seems to be the controlling factor (Sodhi, 2001); for stiff structures ice-induced vibrations do not occur at all. One has to make a choice considering the governing mechanism and each particular choice will yield different predictions. The historically most commonly adopted approaches are defined in Sodhi, (1994), Kärnä et al. (1999), and Määttänen (1999), whereas the approach used in this paper is given in Hendrikse and Metrikine (2015).

The failure maps and ice conditions in this paper reflect model-scale conditions. In full-scale conditions where the ice is often much thicker these failure maps change significantly as pointed out by Blanchet et al. (1988). For thick ice buckling will ultimately disappear from the failure maps as the critical buckling load increases roughly with the third power of the ice thickness, while the axial crushing or creep load increases more or less linearly. Figure 13 shows the failure map for an ice thickness of 1 meter, all other properties given in Table 1. Here it can already be seen that the aspect ratio for which buckling starts to occur shifts to higher values when compared to Figure 4, illustrating the expected change. In full-scale also the elastic modulus of ice is generally much larger than the model-scale value used for the simulations here which additionally increases the critical buckling load.

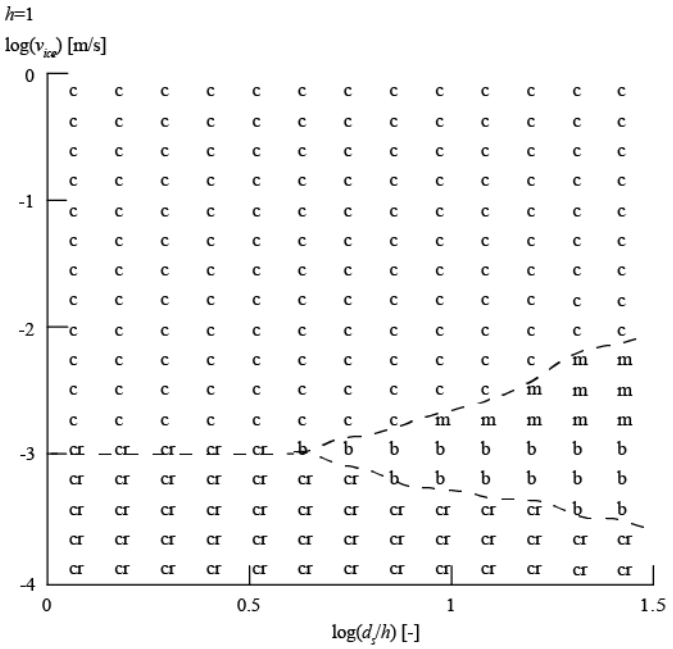

Figure 13 – Numerically generated failure map for 1 meter thick model-ice based on the input values given in Table 1.

Despite the uncertainty with respect to the three conditions identified above, and the outstanding necessity to validate the theories explaining ice-induced vibrations, the results shown in this paper provide insights which are hoped to improve the understanding of ice-induced vibrations. Especially, the obtained results are expected to be useful in conditions of mixed crushing and buckling failure. These conditions are often met in model-scale tests and the authors hope that the model developed in this paper will allow for a more detailed interpretation of model-scale test results for which buckling is observed.

7. CONCLUSION

A model for prediction of the transient ice-structure dynamic interaction has been developed in this paper. The model is applicable to the ice interaction with vertically sided structures and accounts for creep and crushing in the contact zone as well as for the dynamic buckling caused by varying in time in-plane compressive force originated at the contact area. The creep and crushing are modelled by distributed along the contact area phenomenological lumped elements, whereas a wedge beam on elastic foundation is employed to account for flexural ice failure. Special attention in this paper has been paid to the conditions in the regime of mixed crushing and buckling-induced bending failure.

First, the model has been applied under the assumption that the structure is rigid and immovable. It has been shown that the model qualitatively reproduces the transitions between the failure modes of creep, crushing, buckling and mixed crushing and buckling as observed experimentally in laboratory conditions. The dependence of global ice load on velocity for low and high aspect ratios also matches with trends observed in laboratory conditions. Also, the ice load time dependencies predicted by the model have shown to be qualitatively similar to those observed experimentally.

Next, the model has been applied to study ice-induced vibrations in the regime of mixed crushing and buckling of the ice. Results of the study have shown that ice-induced vibrations can develop in such cases as long as the buckling failure does not occur within a period of intermittent crushing or frequency lock-in vibration. This buckling period is predicted to decrease with increasing velocity of the ice and width of the structure.

A combination of parameters of the model has been discovered which predicts the buckling failure of ice on a rigid structure but results in long period of sustained intermittent crushing on a flexible structure of the same size.

This is understood as a consequence of the drops in ice load during intermittent crushing which allow the beam to bend back to the equilibrium in-plane position before the critical bending stress in the beam resulting in bending failure could be reached. Although it is challenging to predict conditions under which such scenario

might occur, the obtained result clearly shows that buckling does not necessarily prevent the occurrence of ice-induced vibrations. The model developed in this paper predicts even that the opposite can happen, namely that ice-induced vibrations may occur under the conditions which would result in buckling should the structure be rigid.

ACKNOWLEDGEMENTS

The authors acknowledge the support from the SAMCoT CRI through the Research Council of Norway and all the SAMCoT partners.

REFERENCES

Bjerkås, M., Meese, A., Alsos, H.S., 2013. Ice-induced vibrations – observations of a full scale lock-in event. Proc. 23rd International Offshore and Polar Engineering Conference (ISOPE), Alaska, USA, 1272-1279.

Blanchet, D., Churcher, A., Fitzpatrick, J., Badra-Blanchet, P., 1988. An analysis of observed failure mechanisms for laboratory, first-year and multi-year ice. Proc. 9th IAHR Ice Symp., Sapporo, Japan, Vol. 2, 89-136.

Hendrikse, H., Metrikine, A., 2015. Interpretation and prediction of ice-induced vibrations based on contact area variation. Int. J. Solids Struct., Vol. 75-76, 336-348.

ISO19906, 2010. Petroleum and Natural Gas Industries— Arctic Offshore Structures. International Organization for Standardization, Geneva.

Jordaan, I.J., 2001. Mechanics of ice-structure interaction. Eng. Fract. Mech., Vol. 68, 1923-1960.

Kärnä, T., Jochmann, P., 2003. Field observations on ice failure modes. Proc. 17th Port Ocean Eng. under Arctic Cond., Trondheim, Norway, Vol. 2, 839-848.

Kärnä, T., Kamesaki, K., Tsukuda, H., 1999. A numerical model for dynamic ice–structure interaction. Comput. Struct. 72, 645–658.

Kerr, A.D., 1978. On the determination of horizontal forces a floating ice plate exerts on a structure. J. Glaciol., Vol. 20, No. 82, 123-134.

Määttänen, M.P., 1999. Numerical model for ice-induced vibration load lock-in and synchronization. Proc. 14th International Symposium on Ice, Potsdam, Vol. 2., 923–930.

Michel, B., Blanchet, D., 1983. Indentation of an S2 Floating Ice Sheet in the Brittle Range. Ann. Glaciol., Vol. 4, 180-187.

Nakazawa, N., Sodhi, D.S., 1990. Ice forces on flat, vertical indentors pushed through floating ice sheets. CRREL Special Report 90-14, 68p.

Nevel, D.E., 1980. Bending and buckling of a wedge on an elastic foundation. Physics and Mechanics of Ice: Symposium Copenhagen, August 6-10, 1979, Technical University of Denmark, Springer Berlin Heidelberg, 278-288.

Palmer, A.C., Goodman, D.J., Ashby, M.F., Evans, A.G., Hutchinson, J.W., Ponter, A.R.S., 1983. Fracture and its role in determining ice forces on offshore structures. Ann. Glaciol., Vol. 4, 216-221.

Schulson, E.M., Duval, P., 2009. Creep and Fracture of Ice. Cambridge University Press, New York

Sodhi, D.S., 1979. Buckling analysis of wedge-shaped floating ice sheets. Proc. 5th Port Ocean Eng. under Arctic Cond. Trondheim, Norway, Vol. 1, 797-810.

Sodhi, D.S., 1991. Ice-structure interaction during indentation tests. Ice Structure Interaction: IUTAM/IAHR Symposium St. John's, Newfoundland Canada 1989, Springer Berlin Heidelberg, 19-640.

Sodhi, D.S., 1994. An ice–structure interaction model. Mech. Geomater. Interfaces, 57–75.

Sodhi, D.S., 1998. Nonsimultaneous crushing during edge indentation of freshwater ice sheets. Cold Reg. Sci. Technol. 27, 179-195.

Sodhi, D.S., 2001. Crushing failure during ice-structure interaction. Eng, Fract. Mech., Vol. 68, 1889-1921.

Sodhi, D.S., Morris, C.E., 1984. Ice forces on rigid, vertical, cylindrical structures. CRREL Report 84-33, December 1984.

Takeuchi, T., Sakai, M., Akagawa, S., Nakazawa, N., Saeki, H., 2001. On the factors influencing the scaling of ice forces. Proc. IUTAM Symposium on Scaling Laws in Ice Mechanics and Ice Dynamics, 149-160.

Timco, G.W., 1980. The mechanical properties of saline-doped and carbamide (UREA)-doped model ice. Cold Reg. Sci. Technol. 3, 45-56.

Timco, G.W., 1987. Indentation and penetration of edge-loaded freshwater ice sheets in the brittle range. Journal of Offshore Mechanics and Arctic engineering, Vol. 198, 287-294.

Timco, G.W., 1991. Laboratory observations of macroscopic failure modes in freshwater ice. Proc. 6th International Cold Regions Engineering Conference, 605-614.

Toyama, Y., Sensu, T., Minami, M. and Yashima, N., 1983. Model tests on ice-induced self-excited vibration of cylindrical structure. Proc. 7th Port Ocean Eng. under Arctic Cond., Helsinki, Finland, Vol. 2., 834–844.

Ziemer, G., Evers, K.-U., 2014. Ice model tests with a compliant cylindrical structure to investigate ice-induced vibrations. Proc. ASME 2014 33rd International Conference on Ocean, Offshore and Arctic Engineering, San Francisco, California, USA, Vol. 10, 8 pages.